Determination of the optimal arrangement of engines along the wingspan

Vladimir Tereshonkov[1*]

[1]Moscow Aviation Institute, Moscow, Russia

Abstract. This article examines the dependence of the loads acting on the wing on the location of the aircraft engines along the wingspan. Based on the obtained dependencies, the optimal position of the power plants along the wing is determined. The values of internal and external force factors acting on the wing are determined by using a simplified wing and engine model in the NX program. Both the loads arising in flight and the factors characteristic of parking on the ground are taken into account. According to the calculations carried out, the optimal position of the external power plant is $z_{en} = 19572\ mm$, and based on optimal position of the engine from the point of view of bending moments was found, equal to $z_{en}^{M_{bend}} = 20973\ mm$. Keywords**:** bending moment, moment of inertia, powerplant, airframe, flight, finite-element (FEM) model.

1 Selection of evaluation criteria

Since the mass of the wing structure depends on the maximum bending moment acting on it, then it should be sought to minimize it. The engine is a concentrated load and unloads the wing in flight, so it is logical to position it as far as possible from the longitudinal axis of the fuselage. However, when parked, the engines load the wing, which is why, on the contrary, it is necessary to reduce the distance between the engines and the longitudinal axis of the fuselage. At the same time, other factors must be taken into account: the distance of the engine from the fuselage contributes to an increase in the longitudinal moment of inertia, which affects the control system and the mass-inertial appearance of the aircraft as a whole. Also, an increase in the separation of engines over a certain value in the event of a failure of one of them requires an increase in the area of the vertical empennage. With the known geometric dimensions of the wing, landing gear and engine nacelles of the aircraft, it is necessary to take into account the possibility of ensuring a roll approach.

It is necessary to determine the optimal, taking into account the limitations, the position of the engines along the wingspan, which would lead to a decrease in the weight of the wing structure [1, 2].

Since the mass of the wing structure is proportional to the bending moment, the bending moment $\boldsymbol{M_{bend}}$. is accepted as a criterion for evaluating the optimal arrangement of the engines $\boldsymbol{z_{en}}$along the span. In this case, the position change relative to the wing will be carried out for the extreme engine at a fixed distance between adjacent engines [3].

* Corresponding author: anatol-06@bk.ru

2 Performing research

As a calculated flight case, we take A' – curvilinear flight at small positive angles of attack with the maximum velocity pressure of a vertical dive. In this case:

$$n_{A'}^{э} = n_{y\,max}^{э} = 2{,}5 \qquad (1)$$

$$q_{A'} = q_{max} \qquad (2)$$

Further, Figures 1-3 show the plots of the distributed aerodynamic load, the distributed load from the wing's own weight and fuel weight, as well as the distributed total load [4].

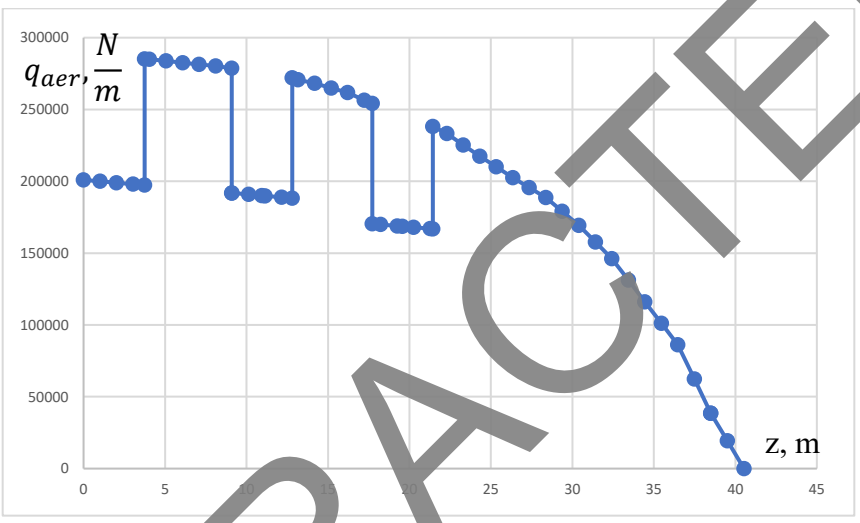

Fig. 1. Plot of distributed aerodynamic load.

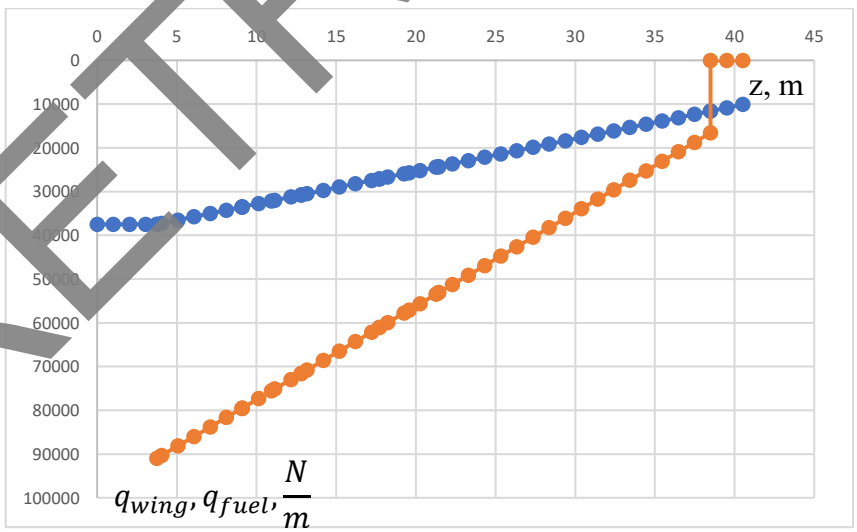

Fig. 2. Plot of loads from own weight and fuel weight.

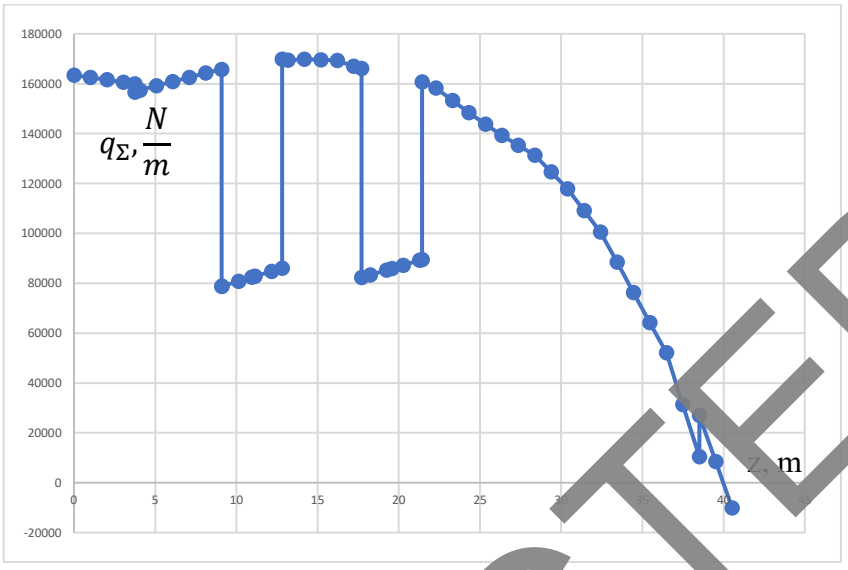

Fig. 3. Plot of the distributed total load.

To carry out the study, the wing with the main power airframe was simplified in Siemens NX (Fig. 4 and 5).

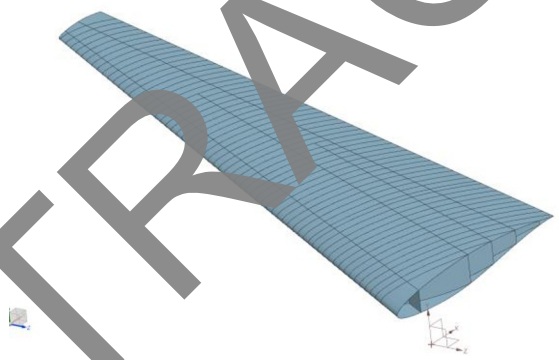

Fig. 4. Wing model of the projected aircraft.

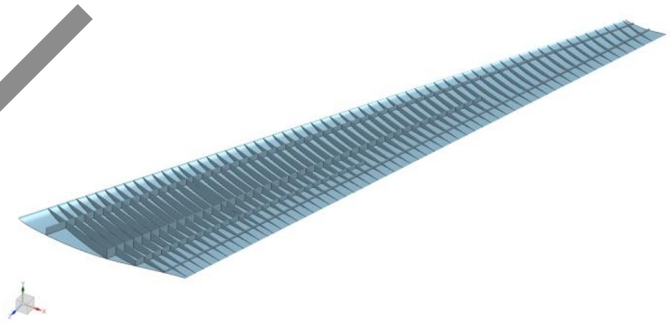

Fig. 5. The main power airframe of the wing.

The engines were modeled as cylindrical bodies (Figure 6). At the same time, five different models were created with different engine locations in terms of wingspan (Figure 7).

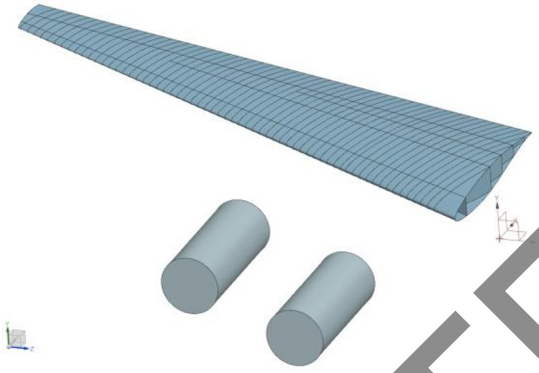

Fig. 6. Detachable wing panel with engines.

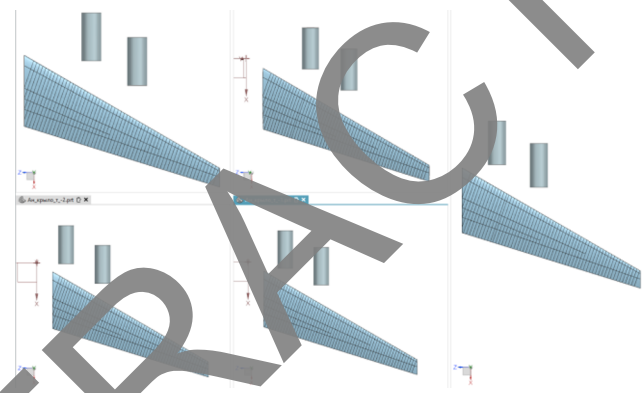

Fig. 7. Engine layout options.

Further, on the basis of these PART-models, finite element models were created (Fig. 8-13). All elements were modeled as 2D bodies. The engines were modeled as 0D elements in the geometric center of the engine models, which were connected to the main structure via 1D connections [5]

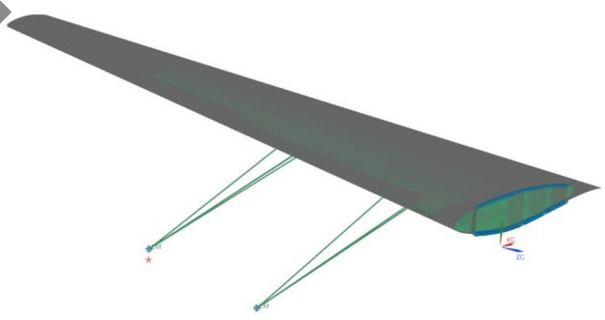

Fig. 8. Finite-element (FEM) model of the wing.

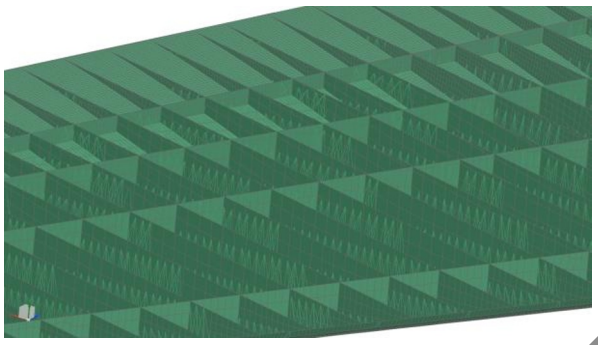

Fig. 9. Finite element 2D regular meshes on the main elements.

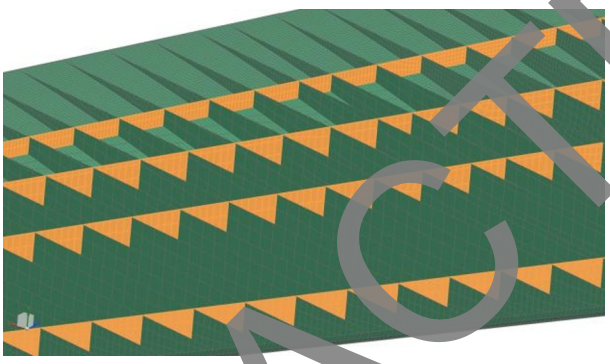

Fig. 10. Finite-element meshes.

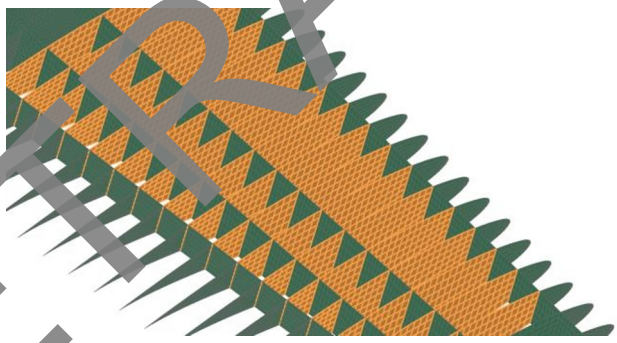

Fig. 11. Finite-element meshes.

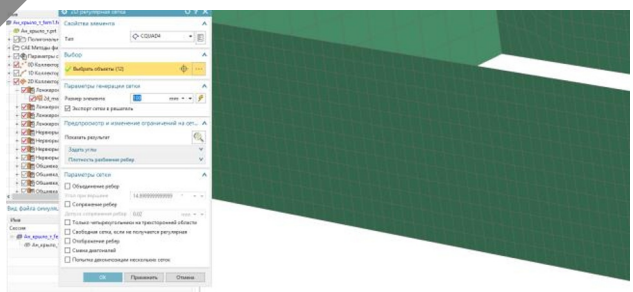

Fig. 12. Finite-element meshes.

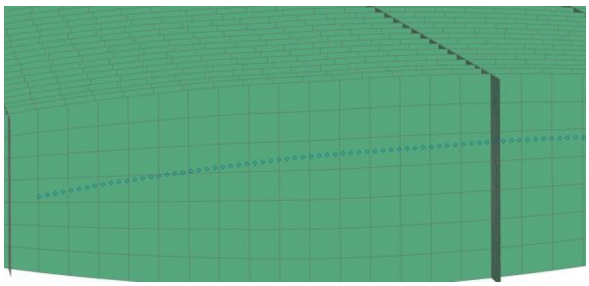

Fig. 13. Finite-element meshes.

Next, a SIM model was created (Fig. 14). To apply loads, RBE2 elements were created, rigidly connected to the upper and lower surfaces of the wing and oriented parallel to the flow (Fig. 15). Aerodynamic load was applied to these RBE2 elements along their entire length, as well as loads from the mass of the wing structure and fuel (Fig. 16-18). Concentrated loads from the engines were applied in concentrated masses (Fig. 19). Restrictions were imposed as a seal at the points of connection of the glasses with the center section (Fig. 20) [6]

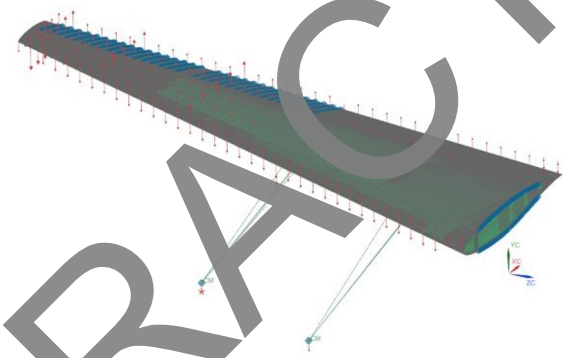

Fig. 14. SIM-model of the wing.

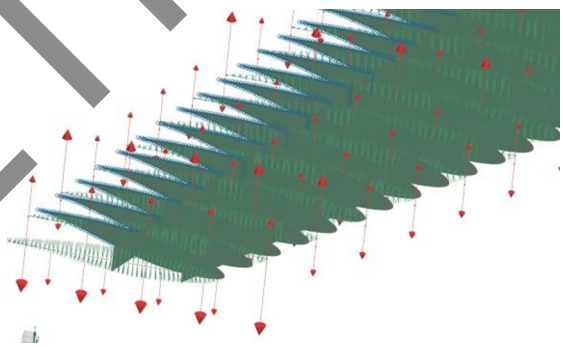

Fig. 15. RBE2 elements for applying loads.

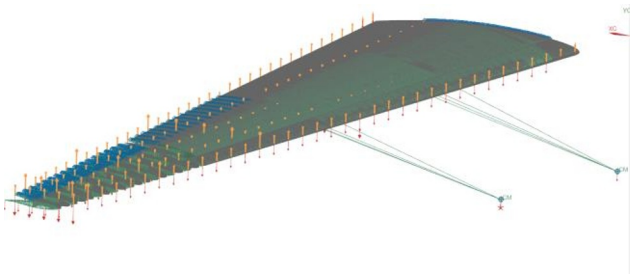

Fig. 16. Aerodynamic load applied to the wing.

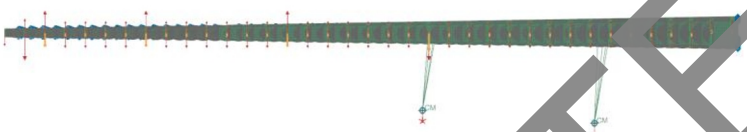

Fig. 17. The load from the mass of the structure applied to the wing.

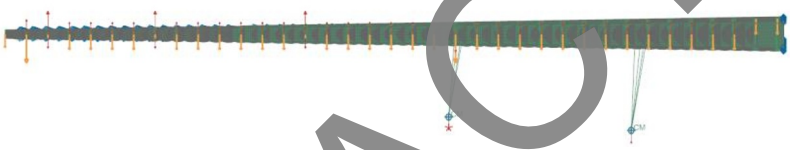

Fig. 18. The load from the fuel of the structure applied to the wing.

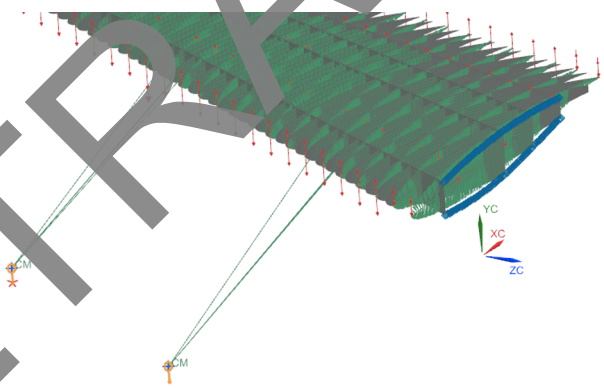

Fig. 19. Concentrated loads from the mass of engines.

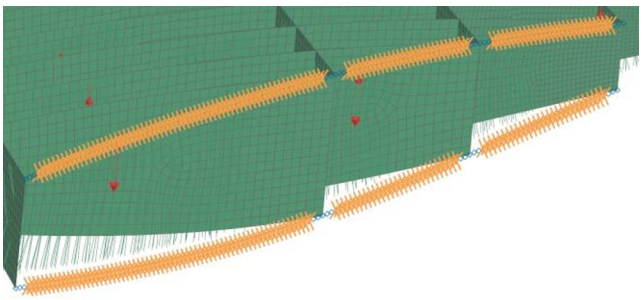

Fig. 20. Sealing at the points of detachable wing panel of the glasses with a center section.

During the calculations, the bending moment values were taken at eight nodes, from which the maximum value for this calculation case was selected (Fig. 21). The values of the bending moment in the nodes, depending on the design case, are summarized in Table 1, and Fig. 22-25 for clarity show the deformations of the wing from the applied loads for different design cases with different engine locations.

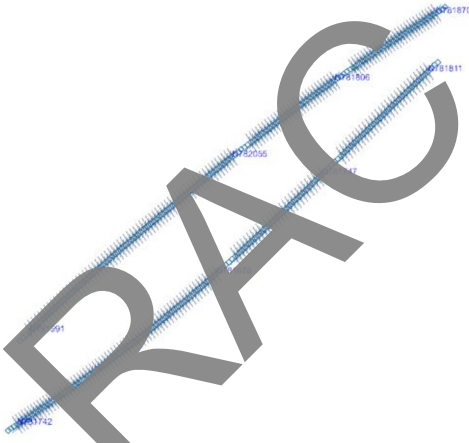

Fig. 21. Nodes where bending moment values were taken.

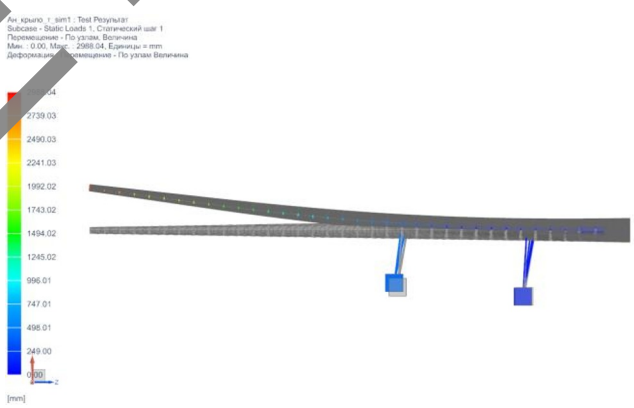

Fig. 22. Deformations for the flight design case with an average arrangement of engines.

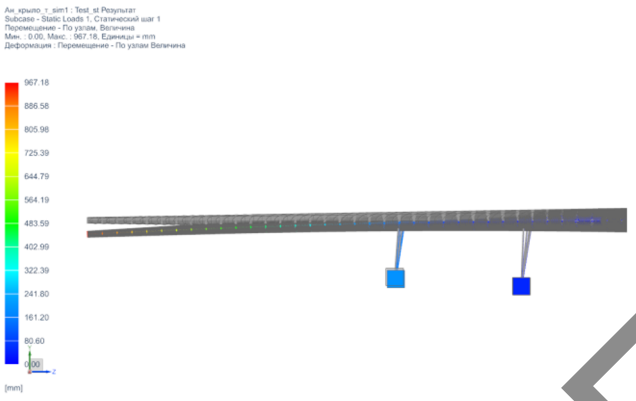

Fig. 23. Deformations for the parking design case with an average arrangement of engines.

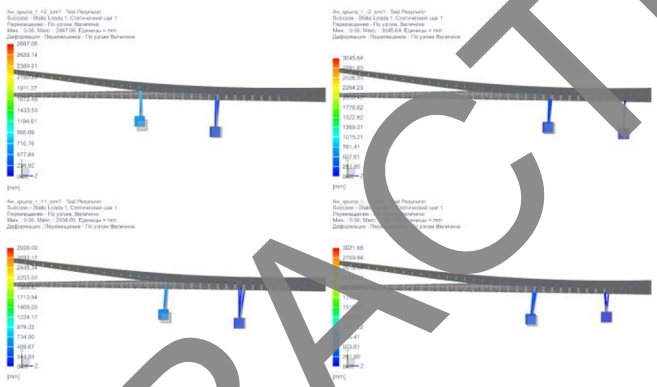

Fig. 24. Deformations for flight cases.

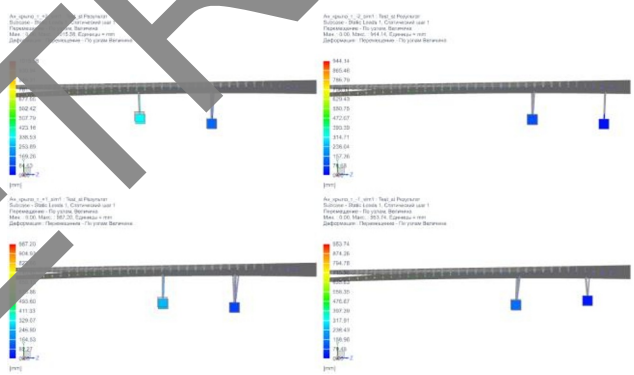

Fig. 25. Deformations for parking case.

Table 1. Bending moments in nodes.

Node		781991	782055	781806	781870	781742	781678	781747	781811
Case	z_{en}, mm	$M_{bend}, N \cdot mm$							
flight	15550	2405440	-628125	-4474090	2405440	2200130	-1227010	-3902510	-7157250
parking		-78891,5	1133810	1654490	1999730	-49255,6	1334010	1468530	2014680
flight	17525	2335610	-693183	-4449700	-7021770	2135910	-1277890	-3882430	-7074090
parking		-106825	1107790	1664250	2032910	-74941,2	1313650	1475430	2047940
flight	19572	2301410	-733368	-4442290	-6,98566	2104970	-1303510	-3882390	-7038270
parking		-120502	1091720	1667210	2047350	-87318,7	1303410	1476570	2062270
flight	22250	2232310	-803623	-4421200	-6906330	2041520	-1354400	3868940	-6959000
parking		-148143	1063610	1675650	2079090	-112700	1283050	1481950	2093980
flight	25000	2161370	-875755	-4399530	-6824880	1976370	-1406650	-3855140	-6877630
parking		-176520	1034760	1684310	2111670	138758	1262150	1487470	2126530

The maximum values of bending moments for each design case at different engine positions are given in Table 2

Table 2. Maximal bending moments in nodes.

z_{en}, mm	Case	$M_{bend}, N \cdot mm$
15550	flight	7157250
	parking	2014680
17525	flight	7074090
	parking	2047940
19572	flight	7038270
	parking	2062270
22250	flight	6959000
	parking	2093980
25000	flight	6877630
	parking	2126530

The resulting dependencies are plotted on one graph (Fig 26).

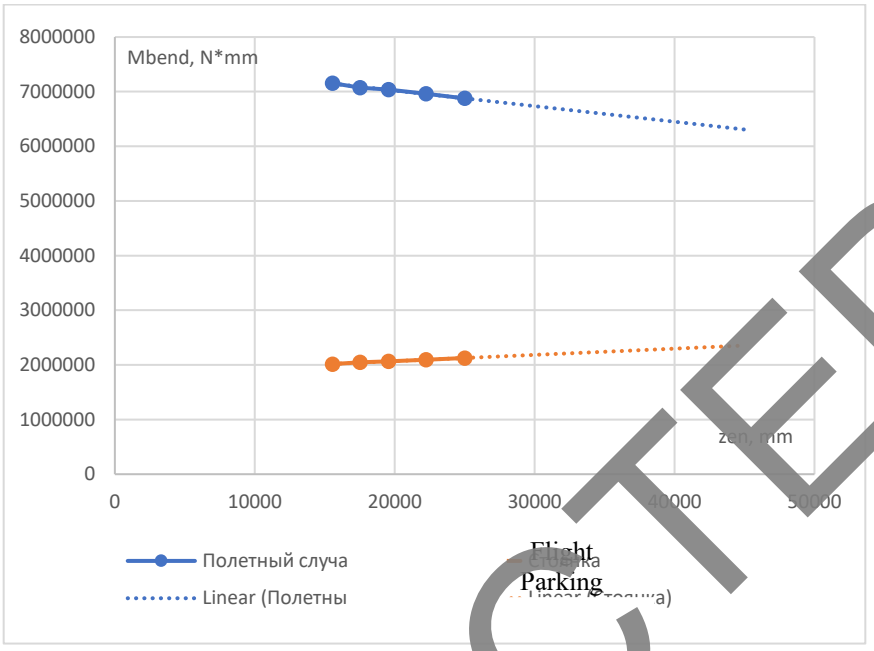

Fig. 26. Maximum bending moments in the detachable wing panel structure depending on the position of the engine for different cases.

Since the obtained dependences do not have an explicit intersection, we use the given values to find the optimal position of the engines:

$$m_i = \frac{M_{bend\ i}}{M_{bend\ max}} \qquad (3)$$

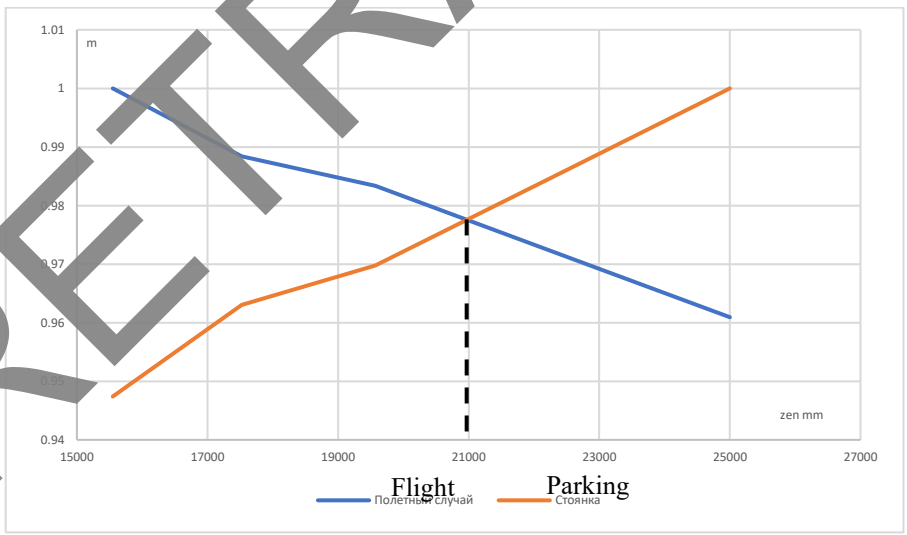

Fig. 27. The given values of moments.

According to the graph, the optimal position is at a distance of $z_{en}^{M_{bend}} = 20973\ mm$.

Consider the first limitation related to the influence of the position of the engines on the longitudinal moment of inertia. The moment of inertia of the power plant relative to the longitudinal axis of the aircraft can be written as

$$J_{x\,pp} = J_{x1} + J_{x2}, \qquad (4)$$

where J_{x1}, J_{x2} are the moments of inertia of the internal and external engines relative to the longitudinal axis of the aircraft.

$$J_{x1} = J_1 + m_{en} {z_1}^2 \qquad (5)$$

$$J_{x2} = J_2 + m_{en} {z_2}^2 \qquad (6)$$

where $J_1 = J_2 = \frac{1}{2} m_{en} \left(\frac{D_{en}}{2}\right)^2$ are the intrinsic moments of inertia of the internal and external engine.

Then the moment of inertia of the power plant can be written as

$$J_{x\,pp} = m_{en} \left(\frac{D_{en}}{2}\right)^2 + m_{en}(z_2 - \Delta z)^2 + m_{en} {z_2}^2 \qquad (7)$$

Here is accepted:

$$z_1 = z_2 - \Delta z \qquad (8)$$

According to this dependence, the moment of inertia of the power plant relative to the longitudinal axis OX of the aircraft depends on the coordinate of the engine squared (Fig. 27).

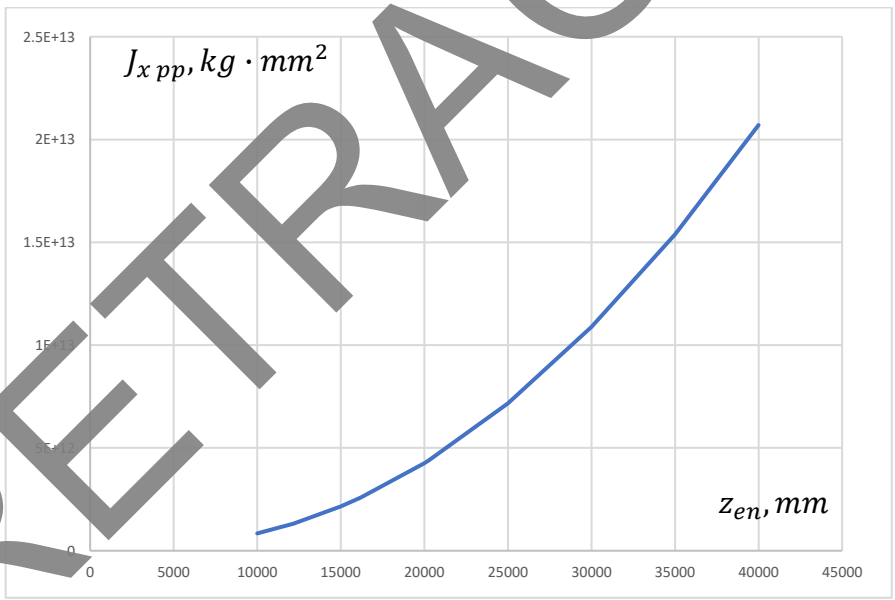

Fig. 28. Dependence of the moment of inertia of the power plant on the coordinate of the engine.

Since the bending moment and the moment of inertia have different dimensions, it is impossible to compare them directly [7]. But you can compare them qualitatively by using the following criterion:

$$K = a_1 M_{bend} + a_2 J_{x\,pp}, \qquad (9)$$

where $a_1 = 3{,}5;\ a_2 = 2 * 10^{-7}$

Let's build this dependence using the already available values:

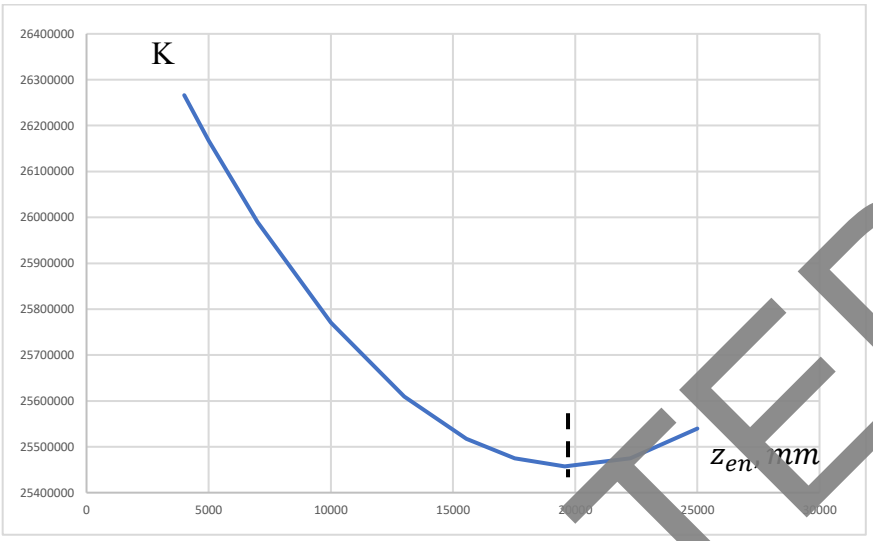

Fig. 29. A complex criterion for assessing the impact on the moment of inertia.

According to this dependence, the optimal position of the engine will be at a distance of $z_{en}^{Jx\,pp} = 19900\ mm$.

Now let's consider the limitation associated with the failure of one engine with the possibility of maintaining stability and controllability and continuing the flight.

The condition for balancing the aircraft in the design mode has the form:

$$m_y^{\delta_r}\delta_{r\,lim} + m_{y\,des} = 0 \quad (10)$$

where $m_y^{\delta_r}$ is the rudder efficiency coefficient; $\delta_{r\,lim}$– the maximum deviation of the rudder.

In case of engine failure (at β=0):

$$m_{y\,des}^{fail} = \frac{P_{fail} z_{en}^{fail}}{qSl} = 0 \quad (11)$$

where P_{fail} is the engine thrust (to failure); z_{en}^{fail} – the shoulder of the failed engine.

$$m_y^{\delta_r} = m_{y\,ve}^{\beta} n_r \quad (12)$$

where $m_{y\,ve}^{\beta}$– derivative m_y^{β}, taking into account the influence of vertical empennage; $n_r = \frac{c_{z\,ve}^{\delta_r}}{c_{z\,ve}^{\beta}}$ is the relative efficiency coefficient of the rudder, at subsonic speed $n_r = \sqrt{\overline{S_r}}$;

$\overline{S_{\text{рн}}} = \frac{S_{\text{рн}}}{S_{\text{во}}}$ – the proportion of the area occupied by the rudder.

$$m_{y\,ve}^{\beta} = A_{ve} c_{z\,ve}^{\beta} K_{ve}\left(1 - \varepsilon_{ve}^{\beta}\right) \quad (13)$$

where K_{ve} is the coefficient of flow deceleration in the vertical empennage area, can be taken $K_{ve} \approx K_{he}$;

ε_{ve}^{β} is the derivative of the average height of the vertical empennage of the angle of the lateral bevel of the flow.

Then substituting expressions into the balancing condition, we get

$$A_{ve} c_{z\,ve}^{\beta} K_{ve}\left(1 - \varepsilon_{ve}^{\beta}\right)\sqrt{\overline{S_r}}\,\delta_{r\,lim} + \frac{P_{fail} z_{en}^{fail}}{qSl} = 0 \quad (14)$$

Where from

$$z_{en}^{fail} = \frac{-A_{ve}c_{z\,ve}^{\beta}K_{ve}\left(1-\varepsilon_{ve}^{\beta}\right)\sqrt{\overline{S_r}}\delta_{r\,lim}qSl}{P_{fail}} \quad (15)$$

Partial derivative $c_{z\,ve}^{\beta}$can be assumed with sufficient accuracy for practice to be equal to $c_{z\,ve}^{\beta} \approx -c_{ya\,ve}^{\alpha}$. With approximate calculations, the value of ε_{ve}^{β} can be neglected. Then

$$z_{en}^{fail} = \frac{-A_{ve}\left(-c_{ya\,ve}^{\alpha}\right)K_{he}\sqrt{\overline{S_r}}\delta_{r\,lim}qSl}{P_{fail}} \quad (16)$$

The second limitation is related to the angle of roll, which is acceptable when landing the aircraft. For heavy aircraft, in the case when the angle of attack is equal to the landing angle, the permissible roll angle may be 4 °. Then, when the transport aircraft is parked, the angle ε will be 8° (Figure 30).

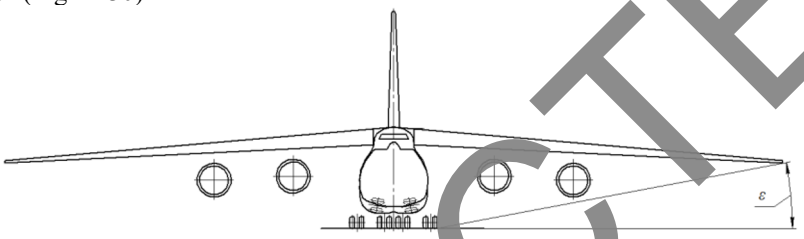

Fig. 30. Determination of the position of the runway surface in relation to the wing tips during landing.

Geometric constructions have shown that in this case the maximum coordinate of the engine can be:

$$z_{en}^{cr} = 26,295\ m \quad (17)$$

3 Conclusions

During the layout, using the similarity parameter, the position of the external motor $z_{en} = 19572\ mm$ was assumed. In the course of the study, the optimal position of the engine from the point of view of bending moments was found, equal to $z_{en}^{M_{bend}} = 20973\ mm$, the error between the received and accepted positions is $\Delta = 6{,}680\%$. At the same time, the adopted provision satisfies the considered restrictions [8, 9, 10].

References

1. D. Strelets, Y. Popov, D. Shavelkin, S. Serebryansky Structural design of airframe units: Didactical Guidelines for preparation of bachelor's graduation thesis in specialization 24.03.04 "Aircraft engineering". – M.: Editus, 146 (2023).
2. P. Orlov P Fundamentals of design: A reference manual. In 2 books. Book 1 and 2. 3rd ed., corrected- M:. Mechanical engineering (1988)
3. F. Lange, R. Rudnik, CEAS Aeronaut J. **12**, 135–146 (2021)
4. I. Konstantinov, V. Tereshonkov, *Development Of A Model For Analyzing The Impact Of Configuration Integrity Loss On The Aircraft Product Cycle Time Duration*, Journal Of Physics: Conference Series 19. "19th International Conference "Aviation and Cosmonautics", AviaSpace 2020" T. 1925. 2021. Publishing Ltd. 19th International

Conference On Aviation And Cosmonautics, Aviaspace 2020 Moscow, 23–27 Nov (2020).

5. B. Safoklov, D. Prokopenko, Y. Deniskin, M. Kostyshak, Transportation Research Procedia, **63**, 1534-1543 (2022)
6. S. Strelets, S. Kantimirov, D. Prokopenko, AIP Conf. Proc. **3021**, 020022 (2024)
7. V. Bekhmetyev, V. Tereshonkov, V. Lepeshkin, Lecture Notes In Electrical Engineering **857** LNEE. 290-299 (2022)
8. D. Strelets, S. Serebrynsky, M. Shkurin, *Concept Of Creation Of A Digital Twin In The Uniform Information Environment Of Product Life Cycle*. In Proceedings Of 2020 13th International Conference Management Of Large-Scale System Development, MLSD (2020)
9. I. Konstantinov, V. Kaigorodova, D. Shavelkin *Methodology for Formation of an Optimized Verification, Validation and Integration Program for an Aircraft Based on Models of Its Architecture*, In Proceedings of the International Conference on Aerospace System Science and Engineering, 25-431 (2021)
10. O. Dolgov, D. Prokopenko, A. Kolosov, I. Abrosimova, Research Procedia **63(2),** 1639-1659, (2022)